Supporting Information for

Cellular Internalization of Polypeptide-Based Nanoparticles: Effects of Size, Shape and Surface Morphology

Jiaxiao Xue, Zhou Guan, Xingyu Zhu, Jiaping Lin,[*] Chunhua Cai,[*] Xiao Jin, Yongsheng Li, Zhaoyang Ye, Wenjie Zhang, and Xinquan Jiang[*]

J. Xue, Z. Guan, X. Zhu, Prof. J. Lin, Dr. C. Cai, X. Jin, Prof. Y. Li, Dr. Z. Ye
Shanghai Key Laboratory of Advanced Polymeric Materials
State Key Laboratory of Bioreactor Engineering
Key Laboratory for Ultrafine Materials of Ministry of Education
School of Materials Science and Engineering
East China University of Science and Technology
Shanghai 200237, China
E-mail: jlin@ecust.edu.cn; caichunhua@ecust.edu.cn

Dr. W. Zhang, Prof. X. Jiang
Department of Prosthodontics
Ninth People's Hospital
Shanghai Jiao Tong University School of Medicine
639 Zhizaoju Road, Shanghai 200011, China
E-mail: xinquanj@aliyun.com

Contents

1. Experimental Section

1.1 Reagents and materials

α-Methoxy-ω-amino poly(ethylene glycol) (mPEG-NH$_2$, M_n = 5,000) was purchased from Sigma-Aldrich. Before use, the mPEG-NH$_2$ macroinitiator was dried by dissolving in toluene and then toluene was removed in high vacuum. *n*-Hexane and 1,4-dioxane (analytical grade) were refluxed with sodium and distilled immediately before use. Acetic ether was refluxed and distilled with calcium hydride. Dialysis bag (Membra-cel, 3,500 molecular weight cutoff) was obtained from Serva Electrophoresis GmbH. All the other reagents were purchased from Adamas-beta and used without further purification. Deionized water was made from a Millipore Super-Q Plus Water System to a level of 18.2 MΩ cm resistance.

1.2 Synthesis of polymers

γ-Benzyl-L-glutamate-*N*-carboxyanhydride (BLG-NCA) was synthesized according to the literature procedure.[S1,S2] Poly(γ-benzyl-L-glutamate) (PBLG) homopolymers and poly(γ-benzyl-L-glutamate)-*block*-poly(ethylene glycol) (PBLG-*b*-PEG) block copolymers were obtained from ring-opening polymerization of BLG-NCA initiated respectively by triethylamine and mPEG-NH$_2$ with 1,4-dioxane as solvent. After 3 days, the viscous reaction mixture was poured into anhydrous ethanol and precipitated. The product was dried under vacuum and then purified twice by repeating the dissolution and precipitation operation.

To label the PBLG-*b*-PEG block copolymer with fluorescein isothiocyanate (FITC), we firstly modified the PBLG blocks with ethylenediamine. The PBLG-*b*-PEG block copolymer (0.3 g) was dissolved in 50 mL *N,N′*-dimethylformamide (DMF), followed by the addition of 1 g 2-hydroxypyridine and 3 mL ethylenediamine. The solution was stirred and reacted for 20 min at 40 ℃. After precipitating with anhydrous ethanol and filtration, the amino modified product P(BLG-*co*-ELG(NH$_2$))-*b*-PEG block copolymer was collected and dried under vacuum. Then the obtained amino modified product (0.2 g) was dissolved in 25 mL DMF. Subsequently, 0.1 g FITC was added to the solution with several drops of trimethylamine. The mixed solution was stirred overnight in dark at room temperature. After precipitating with anhydrous ethanol and filtration, the product PBLG(FITC)-*b*-PEG was collected and dried under vacuum.

Polystyrene (PS) was synthesized by atom transfer radical polymerization (ATRP) with ethyl 2-bromoisobutyrate (EtBriB) as initiator according to literature.[S3]

1.3 Polymer characterizations

The molecular weights of PBLG-based block copolymers were estimated using ^{1}H NMR measurement (Avance 550, Bruker, CDCl$_3$/TFA-d or DMSO-d_6 as solvent). Figure S1 shows the ^{1}H NMR spectra of (a) PBLG-b-PEG, (b) P(BLG-co-ELG(NH$_2$))-b-PEG, and (c) PBLG(FITC)-b-PEG block copolymers. For the PBLG chain of the block copolymer, the typical proton signals originated from methylene group of benzyl (δ = 5.1 ppm) and methylene group of block backbone (δ = 4.6 ppm) can be seen in Figure S1a, and that of the methyl group of the PEG block also appears in the spectrum (δ = 3.7 ppm), indicating the successful synthesis of the block copolymer PBLG-b-PEG. For the block copolymer, as the molecular weight of PEG segment is known (M_n = 5,000), the degree of polymerization (DP) of PBLG segment can be calculated by the intensity ratio of methylene group of BLG units (δ = 5.1 ppm) to the methyl group of PEG block (δ = 3.7 ppm).[S4,S5] According to the NMR analysis, the DP of the PBLG block is calculated to be 168, and the M_n value of PBLG-b-PEG block copolymer was calculated to be 41,800.
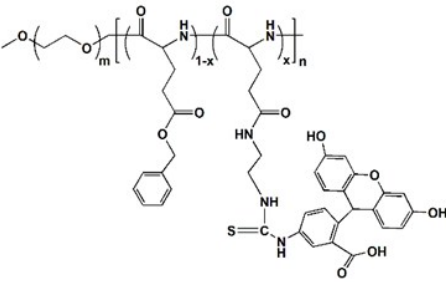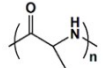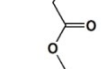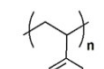
For the P(BLG-co-ELG(NH$_2$))-b-PEG copolymer, the peak of imino group (δ = 8.0 ppm) comes up, indicating that the modified copolymer was obtained (Figure S1b). And the number of the attached amine group for each PBLG block is calculated to be 16. When the FITC group is attached on the side chain of the block copolymer, the peak at 6.5 ppm appears in the spectrum (Figure S1c). By comparing the peak intensity of the methine group of PBLG chain (δ = 3.9 ppm) with that of the FITC group (δ = 6.5 ppm), the number of the attached FITC group is calculated to be 7. Thus, the fluorescent labelled copolymer was successfully synthesized.

The molecular weights of PBLG and PS homopolymers were measured from gel permeation chromatography (PL-GPC, Varian, PMMA as standard). The structure information of the block copolymers and the homopolymers are provided in Table S1.
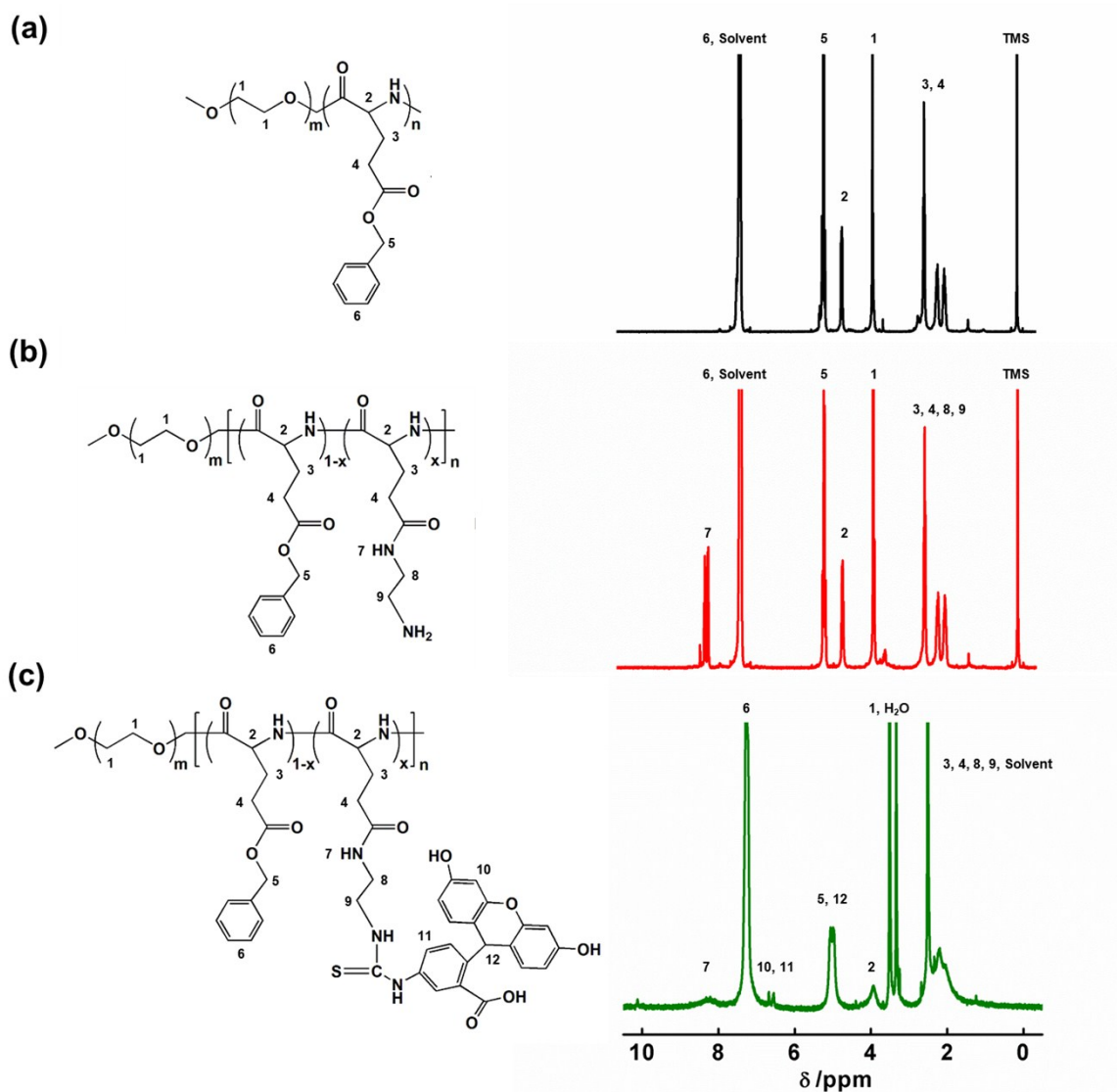
Figure S1. ^{1}H NMR spectra of (a) PBLG-*b*-PEG in CDCl$_3$/TFA-*d*, (b) P(BLG-*co*-ELG(NH$_2$))-*b*-PEG in CDCl$_3$/TFA-*d*, and (c) PBLG(FITC)-*b*-PEG in DMSO-*d*$_6$.

Table S1. Polymer characterizations

Molecular structure	Sample	M_n^a ($\times 10^3$ g/mol)	PDI[b]
	PBLG(FITC)-*b*-PEG	PBLG(FITC): 38.7 PEG: 5	1.25
	PBLG-1	28	1.19
	PBLG-2	118	1.21
	PBLG-3	300	1.22
	PS-1	10	1.21
	PS-2	19.4	1.15

[a] For the block copolymers, the M_n value of PEG segment was known, and the M_n of polypeptide blocks were derived according to ^{1}H NMR spectra. The M_n of PBLG and PS homopolymers were measured from GPC testing.

[b] The PDI values of the polymers were obtained from GPC testing.

1.4 Preparation of self-assembled NPs

Firstly, PBLG or PS homopolymers and PBLG(FITC)-*b*-PEG block copolymers were separately dissolved in corresponding solvents. The polymer concentration of the stock solutions is 0.6 g/L. Then, 8 mL block copolymer solutions and 2 mL homopolymer solutions were mixed together. 2.5 mL deionized water was added to the mixed solutions at a rate of 0.02 mL/s with vigorous stirring to prepare the NPs.

For the helical rods, PBLG(FITC)-*b*-PEG and PBLG were dissolved in tetrahydrofuran (THF)/*N,N'*-dimethylformamide (DMF) mixture solvent (3:7, v:v). The molecular weight (M_n) of PBLG is chose as 118,000 and 300,000 for short and long helical rods, respectively. The striped spheres were prepared by the mixture of PBLG(FITC)-*b*-PEG/PS. For the small one, the mixture of PBLG(FITC)$_{38,700}$-*b*-PEG$_{5,000}$/PS$_{10,000}$ (the subscript denotes the molecular weight of the polymer) was dissolved in THF/DMF mixture solvent (7:3, v:v). In the preparation of the large striped sphere, the mixture of PBLG(FITC)$_{38,700}$-*b*-PEG$_{5,000}$/PS$_{19,400}$ was dissolved in THF/DMF mixture solvent (3:7, v:v). In the preparation of the small smooth sphere, the mixture of PBLG(FITC)$_{38,700}$-*b*-PEG$_{5,000}$/PBLG$_{28,000}$ was dissolved in THF. In order to prepare smooth spheres with larger size, the mixture of PBLG(FITC)$_{38,700}$-*b*-PEG$_{5,000}$/PS$_{19,400}$ was dissolved in DMF.

Subsequently, the solution was dialyzed against deionized water for 3 days to remove the organic solvents. All the experimental procedures, including the processes of adding water and dialysis were performed at 20 ºC. All the prepare processes were shielded from light. Before incubating with NIH3T3 cells, the NP solutions were stabilized for at least 5 days. The fluorescence of the NPs was confirmed by confocal laser scanning microscopy (CLSM) measurement.

1.5 Characterization methods of the NPs

Scanning electron microscopy (SEM). The morphologies of NPs were observed by field emission SEM (S4800, HITACHI) operated at an accelerating voltage of 15 kV. The samples were prepared by placing drops of solution on a copper grid coated with carbon film and then dried at room temperature. Before observations, the samples were sputtered by gold.

Dynamic light scattering (DLS). DLS was measured by an LLS spectrometer (ALV/CGS-5022F) equipped with an ALV-High QE APD detector and an ALV-5000 digital correlator using a He-Ne laser (the wavelength $\lambda = 632.8$ nm) as the light source. All the measurements were carried out at 20 °C. The scattering angle is 90°. The hydrodynamic radius (R_h) of the NPs can be obtained from the DLS testing.

Zeta potential measurement. The zeta potentials (ζ) of the six types of NPs were measured using a Malvern Zetaseizer 3000HS in Dulbecco's modified Eagle medium (DMEM) with polymer concentration of 0.2 g/L at 20 °C. Each sample was measured five times.

Flow cytometry measurement. After the cells were incubated with the NPs for 6 hours, Cells were collected and rinsed three times with phosphate buffer saline (PBS, pH = 7.4). And then, the concentration of cells was adjusted to 5×10^5 cells/500 μL PBS. The cells suspension was measured with a BD FACSCalibur flow cytometer with the excitation wavelength set to be 488 nm.

Inhibition study of internalization. The inhibition studies of internalization were performed as follows. NIH3T3 cells were seeded in 24-well plates at 5×10^4 cells per well in 1 mL of DMEM and cultured at 37 °C in a humidified atmosphere of 5% CO_2 for 24 h. The cells were treated with 0.1% NaN_3 and 50 mM 2-deoxyglucose for 1 h, then the medium was changed to fresh medium containing both the inhibitor and the NPs before further incubation at 37 ºC in a humidified atmosphere of 5% CO_2 for 2 h. Then the media were removed and the cells were rinsed three times with PBS and fixed with 4% formaldehyde for 15 min at 4 °C. The cell nuclei were stained with DAPI (blue fluorescence).

Cytotoxicity measurements. The relative cytotoxicity of the FITC labeled NPs against NIH3T3 cells was estimated by thiazolyl blue tetrazolium bromide (MTT) assay. NIH3T3 cells were seeded into a 96-well plate at a density of 5×10^3 cells per well in DMEM and cultured for 24 h. The aggregate solutions were added and incubated with cells for 8 h. The culture medium was removed and the wells were washed three times with PBS solution, and then 100 μL of a 0.5 g/L MTT solution in PBS was added into each well. After further incubation for 4 h at 37 °C, the medium containing unreacted MTT was removed, and 150 μL of DMSO was added into each well to dissolve the received blue formazan crystals. Finally, the absorbance at 490 nm was measured using a UV-vis spectrometer. The cell viability was calculated as a percentage of absorbance relative to control cells. Each experiment was carried out in septuplicate.

1.6 DLS measurements of the NPs

The hydrodynamic radius (R_h) of the NPs can be measured from DLS. Diffusion coefficient (D_s) is the diffusion rate of particles in solution, that is, particles which have larger diffusion coefficient have faster Brownian movement and larger lag time.[S6] The hydrodynamic radius (R_h) can be calculated with D_s according to Stockes-Einstein equation:

$$D_s = \frac{kT}{f} = \frac{kT}{6\pi\eta R_h}$$

(S-1)

where k is Boltzmann constant, f is frictional coefficient, T is temperature, and η is the viscosity of the solution. It should be noted that the R_h for the helical rod is the radius that is equivalent to the radius of a sphere which has the same frictional coefficient with the helical rod in solution.

Figure S2 shows the hydrodynamic radius distribution of these NPs. As measured by DLS, the helical rod-1 and 2 have the average R_h of *ca.* 111.2 nm and 164.0 nm, respectively. For the striped sphere-1 and 2, the average R_h are *ca.* 112.9 nm and 163.3 nm, respectively. Similarly, smooth sphere-1 and 2 possess the average R_h of *ca.* 114.4 nm and 168.5 nm, respectively. The corresponding polydispersity indices are 0.13, 0.12, 0.10, 0.12, 0.12, and 0.11 for helical rod-1, striped sphere-1, smooth sphere-1, helical rod-2, striped sphere-2, and smooth sphere-2, respectively. The relative low polydispersity indices imply that those NPs are uniform in size.
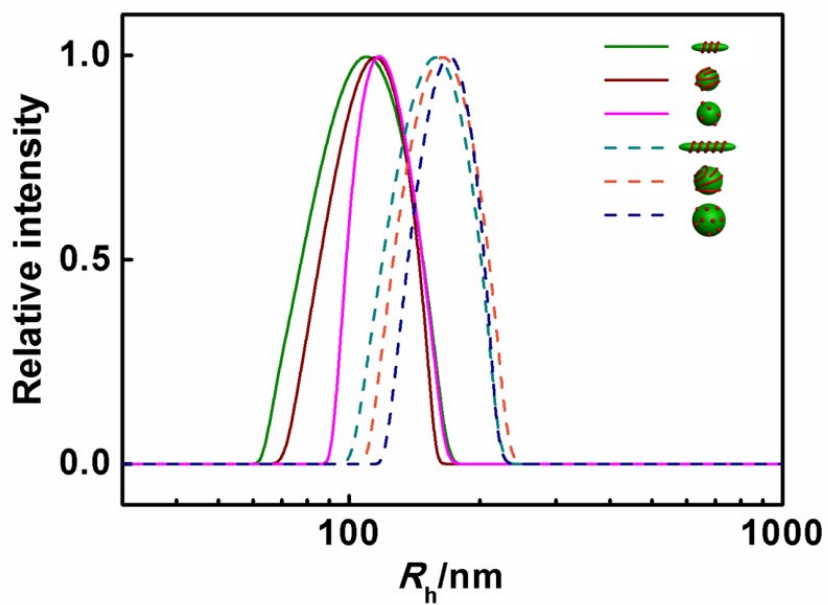
Figure S2. R_h distributions for the self-assembled NPs (scattering angle 90°).

1.7 Observation of cells incubated with NPs

The internalization of NPs usually causes the cell membranes wrinkling and protruding, which can be captured from SEM images of cell surfaces. The cellular internalization of particles comes to a relatively high rate after 8-h incubation, which is chosen as the representative instance to show the influence of internalization process on cell membranes. SEM images of NIH3T3 cells incubated with NPs for 8 h are shown in Figure S3a-h. As shown in Figure S3a and e, cell membrane of control group is relatively flat and smooth. As a result of the cellular uptake of NPs, bumped cell morphologies and protrusions extending from the cell bodies can be observed in the three sample groups (Figure S3b-d). Because the particles are wrapped in membranes, the morphology of the NPs cannot be observed clearly. Figure S3h exhibits 3D overlay CLSM images of NIH3T3 cells incubated with helical rod-2 for 8 h, which convinces that the helical rods have entered into cytoplasm. The corresponding fluorescent image in green channel is shown in Figure S3i which also proves the internalization of NPs. As shown by the profile of fluorescent intensity distribution of one cell (Figure S3k), the NPs mainly concentrate in the cytoplasm and a few still attach to the membrane.
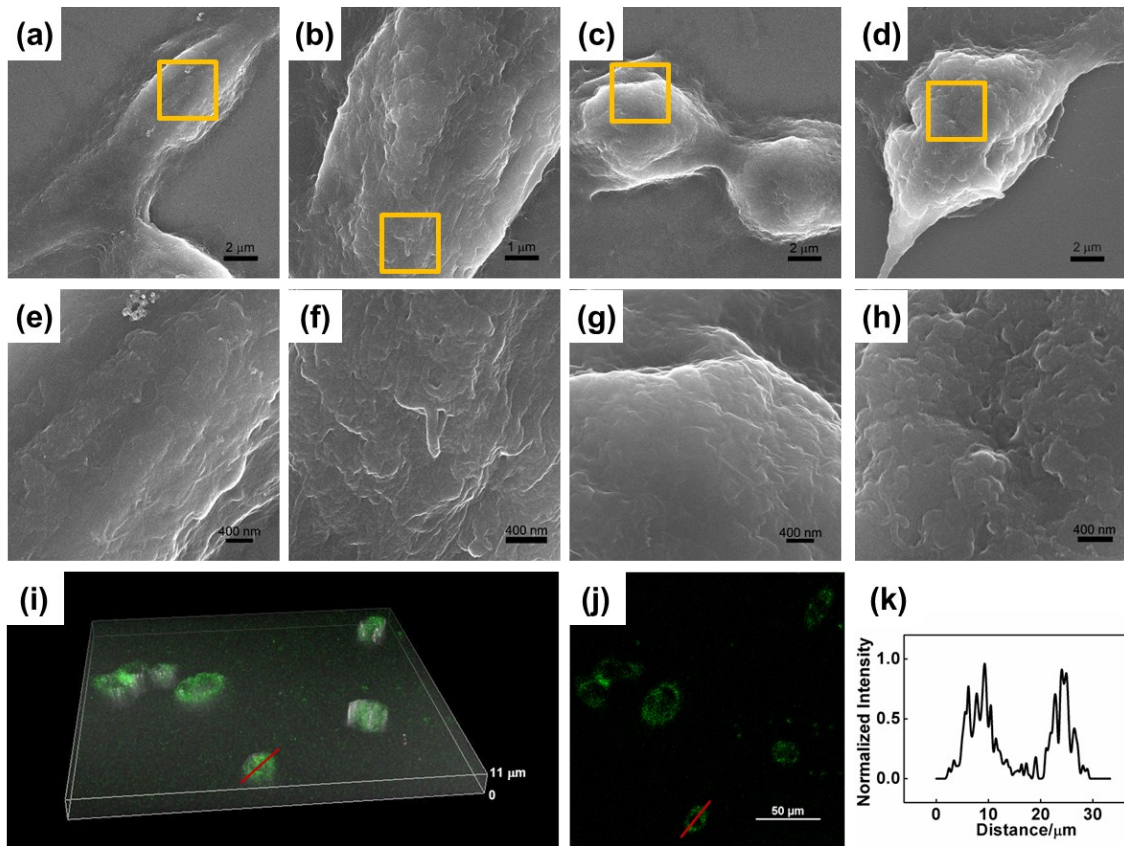
Figure S3. SEM images of NIH3T3 cells after 8-h incubation with NPs: (a) control group without NPs, (b) helical rod-2, (c) smooth sphere-2, and (d) striped sphere-2. (e-h) Magnified images of cells marked with yellow squares in (a-d), respectively. (i) 3D overlay image and (j) CLSM image (green channel) of NIH3T3 cells after 8-h incubation with helical rod-2. (k) Fluorescent intensity distribution of one cell along the red lines in (i) and (j).

2. Simulation Section
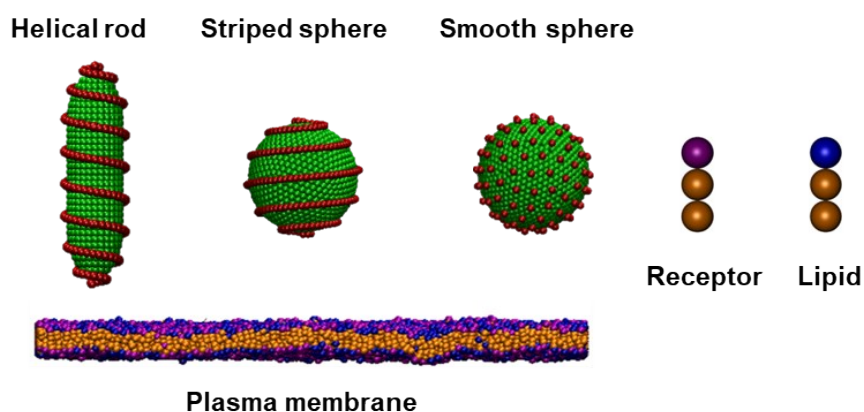
2.1 Coarse-grained simulation model

We provide the simulation morphologies of the three types of NPs as reported in our previous work,[S2] as shown in Figure S4. The template formed by PBLG or PS homopolymers were denoted by blue, while the PBLG-*b*-PEG block copolymer shells or helical strings on the template are denote by green (PBLG) and red (PEG). For reducing the computational cost, the three types of NPs were coarse-grained in the present work. The rod-like and spherical templates were constructed by hydrophobic beads, as shown in Figure S5, denoted by green. Since the distal methoxy group of PEG can binds to the proteins (act as receptors) on the membrane via a weaker hydrophobic interaction or hydrogen bonding, the PEG corona is coarse-grained into ligands on the hydrophobic templates, denoted by red.

In addition, the packing manners of ligands on the template correspond to those in the experiment and mapped from the morphologies simulated in our previous works.[S2,S7] A helical or uniform arrangement was adopted for the helical rod or the smooth sphere, respectively. For the striped sphere, the stripes on the surfaces take a spiral-like structure, which can well represent its main surface morphology observed in the experiments.

The plasma membrane is formed by a certain number of lipids. Each lipid and receptor is coarse-grained into a chain formed by three beads, as can be seen in Figure S5. The first bead of lipid is hydrophilic, and the two tail beads are hydrophobic. Some of the lipids act as receptors. The two tail beads in receptors are the same with those in lipids, while the first beads are different. They can correspond to the proteins on plasma membrane (*e.g.*, cholesterol and transferrin), which can bind to the ligands (denote the distal methoxy group of PEG in experiments) of NPs.[S8]
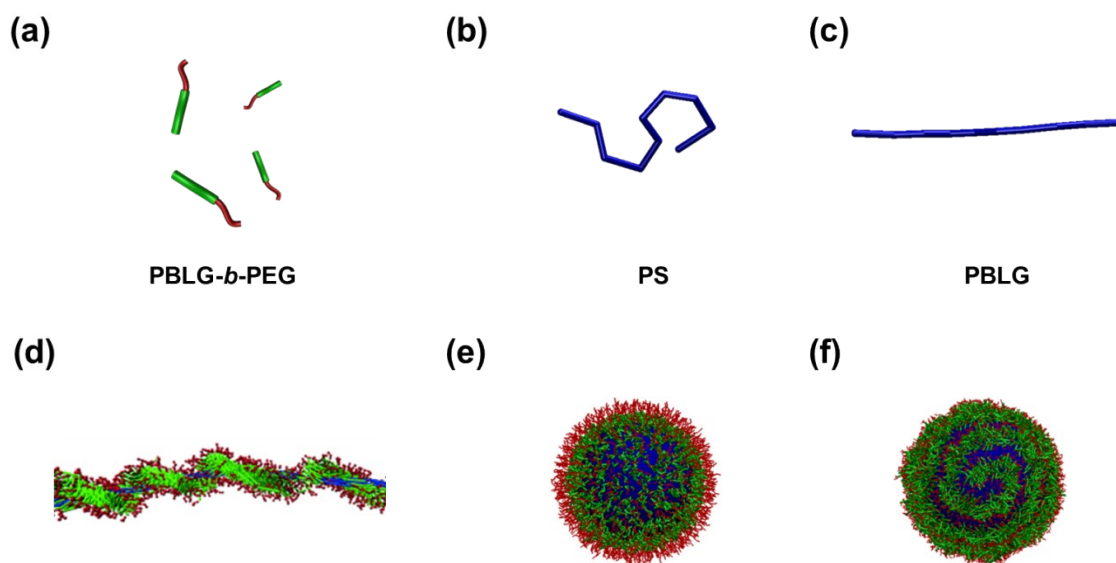
Figure S4. Simulation results of the three types of NPs reported in our previous work. Molecular models of: (a) PBLG-*b*-PEG block copolymer, (b) PS homopolymer, and (c) PBLG homopolymer. (d) rod-like NP with helical surface, self-assembled from PBLG-*b*-PEG/PBLG binary system. (e) spherical NP with smooth surface, self-assembled from PBLG-*b*-PEG/homopolymer (PS or PBLG) binary system. (f) spherical NP with spiral-like surface, self-assembled from PBLG-*b*-PEG/PS binary system. Blue beads denote the PBLG and PS homopolymers, which forming the template, while green and red beads denote PBLG and PEG segment in block copolymers, which forming the strings or shells on the template.[S2]

Figure S5. Coarse-grained models in the simulations. Green and red beads denote the hydrophobic template and hydrophilic strings or shells, respectively, of the NPs in experiments. The orange beads in receptor and lipid correspond to the hydrophobic tails, while the purple and blue beads are hydrophilic heads. The plasma membrane in the system is self-assembled from receptors and lipids.

2.2 Simulation method

The solvent-free method, proposed by Cooke et al., was adopted in the simulations of present work.[S9] This method maintains the principal properties of cell membrane. Because there are no solvent beads in the method, the simulation can be performed efficiently, and greater time and size simulation scale can be realized. This method has been successfully applied to study the endocytosis of NPs.[S10]

In this method, the bonds linking two neighbored beads in lipids or receptors are defined by a finite extensible nonlinear elastic (FENE) potential:

$$U_{\text{bond}}\left(r\right) = -1/2 k_{\text{b}} r_{\text{b}}^2 \ln\left[1-\left(r/r_{\text{b}}\right)^2\right] \tag{S-2}$$

where the k_{b} and r_{b} are the strength of the potential and the maximum extend of bond. Additionally, a harmonic spring potential is applied between the head and second tail beads to maintain straightened shape of lipids:

$$U_{\text{angle}}\left(r\right) = 1/2 k_{\text{a}}\left(r-r_{\text{a}}\right)^2 \tag{S-3}$$

in which k_{a} and r_{a} are the strength of the potential and the equilibrium bond distance. In this model, the potential between all the beads are represented as follows:

$$U_{\text{inter}}\left(r\right) = \begin{cases} 4\varepsilon_0\left[\left(\lambda_{ij}\sigma/r\right)^{12}-\left(\lambda_{ij}\sigma/r\right)^6\right], & r < r_{\text{cut}} \\ -\varepsilon_{\text{atr}}\cos^2\left[\pi\left(r-r_{\text{cut}}\right)/2r_{\text{atr}}\right], & r_{\text{cut}} \le r \le r_{\text{cut}}+r_{\text{atr}} \\ 0, & r > r_{\text{cut}}+r_{\text{atr}} \end{cases} \tag{S-4}$$

The top piece of the function is a Lennard-Jones potential. ε_0 is the interaction strength and set as unit energy in the present work. σ and λ are the length unit and modulus, respectively. r_{cut} denotes the cut-off distance of the first potential. The middle piece of the function represents the attraction between all tail beads of lipids, and the binding between ligands and receptors. ε_{atr} and $r_{\text{cut}} + r_{\text{atr}}$ are the interaction strength and cut-off distance of the second potential.

The simulations were performed under NΣT ensemble (N, Σ, and T denote the number of beads, membrane lateral tension, and system temperature, respectively). A Langevin thermostat, developed by Schneider and coworker was adopted in present simulations to maintain constant temperature.[S11] The beads are coupled to a heat bath and the equations of motion written by:[S12]

$$m_i \mathbf{a}_i = \mathbf{F}_i - \Gamma \mathbf{v}_i + \mathbf{W}_i(t) \qquad (\text{S-5})$$

where m_i, $\mathbf{a}_i$, and $\mathbf{v}_i$ is the mass, acceleration, and velocity of the ith bead. $\mathbf{F}_i$ is force acting on the ith bead, which is calculated by the potential energies consisting of $U_{bond}(r)$, $U_{angle}(r)$, and $U_{inter}(r)$. Γ is friction constant. In the Langevin dynamics, the effect of solvent molecules is implicitly treated by the noise term $\mathbf{W}i(t)$, which can be calculated using the fluctuation-dissipation relation:[S13,S14]

$$\left\langle \mathbf{W}_i(t) \cdot \mathbf{W}_j(t') \right\rangle = 6k_B T \Gamma \delta_{ij}(t - t') \qquad (\text{S-6})$$

In addition, we adopted constant lateral tension condition in the simulations. Here, a modified Berendsen barostat was used to maintain a desired lateral tension.[S15] The simulation box and coordinates of beads were rescaled in the dimensions parallel to the membrane (*i.e.*, x/y dimensions in our simulations) according to the current membrane lateral tension. The scaling factor $\mu_{x/y}$ is given by:

$$\mu_{x/y} = 1 + \frac{dt}{T_p K} \left[\Sigma_0 - \Sigma(t) \right] \qquad (\text{S-7})$$

where dt is the time step, T_p is the relaxation time, K is the compression modulus, Σ_0 is the desired tension. $\Sigma(t)$ is the current membrane lateral tension:

$$\Sigma(t) = -\frac{P_{xx}(t) + P_{yy}(t)}{2} \qquad (\text{S-8})$$

2.3 Parameter setting

Although the simulation system is coarse-grained for the model and parameters, we tried to make the simulation system and experimental system close, by setting the important parameters close to those of experiment systems. The followings are the discussion and explanation on the choice of the important parameters.

Sizes of NPs. We set the size of NPs in the simulations according to the aspect ratio of those in the experiments. For the helical rods in the experiments, the diameter (d) is 105.8±5.2 nm and the length (l) is 457.9±16.7 nm, therefore, the ratio of the diameter to the length is 105.8/457.9 ≈ 1/4. Correspongdingly, in silmulation model, the diameter and the length of the helical rods were set to 8σ and 32σ, respectively. For the striped spheres and the smooth spheres, their radii (r) are 109.4±5.8 nm and 108.5±7.4 nm, respectively, which are close to the diameter of the helical rods (d = 105.8±5.2 nm), therefore, in the simulations the radius of both the striped spheres and the smooth spheres was set to 8σ. All of the NPs were constructed with 1010 hydrophobic (template) and 131 hydrophilic beads (ligands) beads, denoted in green and red, respectively. Keeping the number of ligand beads on each NP fixed at 131, the packing manners of ligands on the surfaces were different. For the rod-like NP, the ligands are helically decorated. And for the striped sphere, the ligand are parked in a spiral-like manner, while for the smooth sphere, the ligands are uniformly packed, as shown in Figure S5.

Sizes of plasma membrane. The membrane was constructed with 4400 lipids, 50% of which were receptors. The initial size of membrane is 70×70 σ^2, where σ denotes the length unit. Using Berendsen barosat (Equations S-7 and S-8), the area of membrane were varied for maintaining a constant tension. The relaxation time T_p and compression modulus K were set to 100 and 0.001, respectively.

Bonding potential. The bonding potentials, including FENE bond potential (Equation S-2) and harmonic spring angle potential (Equation S-3), were applied in the lipids and receptors of plasma membrane. For FENE bond potential, the strength $k_b = 30\varepsilon_0/\sigma^2$ and the maximum extend of bond $r_b = 1.5\sigma$.[S9] ε_0 denotes the energy unit. For the harmonic spring angle potential, the strength $k_a = 10\varepsilon_0/\sigma^2$ and the equilibrium bond distance $r_a = 4\sigma$.

Nonbonding potential. As provided in the Equation S-4, the cut-off distance of the potential $r_{cut} = 2^{1/6}\lambda\sigma$. The values of λ_{HH} and λ_{HT} were both set as 0.95, where the letters H and T denote the head/ligand and tail beads of phospholipids, respectively. For other beads, the values of λ were all set to 1. For tail beads, $\varepsilon_{atr} = \varepsilon_0$, and $r_{atr} = 2.53\sigma$, which are supposed to be the optimal values for maintaining a plasma membrane.[S1] The ligands on NP and the receptors on membrane in the simulations denote the free end of PEG segments and the protein, respectively, in the experiments. Since the distal methoxy group of PEG segments can bind to the proteins on membrane with a strength of 2~7 $k_B T$,[S16] we set the receptor-ligand binding strength to $5\varepsilon_0$ ($1\varepsilon_0 = 1$ $k_B T$) in the simulations. The value of r_{atr} was set to 1.45σ, which has been used as a proper value in the simulation work by Vácha *et al.*[S10]

Through such choices of parameters, we found the simulation results are able to capture the characteristics of the experimental systems. These setting can guarantee a qualitative consistent between simulations and experiments, although the quantitative match is difficult to obtain due to the limitation of current computation ability.[S17]

2.4 Simulation system

The simulations were performed under NΣT ensemble (N, Σ, and T denote the number of beads, membrane lateral tension, and system temperature, respectively). The system contains a bilayer plasma membrane and a NP decorated with ligands, as shown in Figure S5. The simulation box is 70×70×200 σ^3 in size. The CGMD simulations were run for at least $2\times10^6 dt$, where the time step dt was set to 0.01τ. The initial distance between the bottoms of NPs and membrane (d_{NM}) were set to 0σ, and the major axis of NP is vertical to the membrane ($\theta_0 = 0$), unless otherwise specified. In the investigation of cellular uptake percentages as a function of time, we performed the simulations 20 times for each NP under various d_{NM}. d_{NM} was ranged from 0 to 20σ, and each NP was given an initial velocity of -$5\sigma/\tau$ in z direction towards the membrane, so that all the NPs can contanct with the membrane.

2.5 Cellular internalization of NPs with large sizes

In the main text, we studied the cellular internalizations of the three types of NPs having smaller sizes via simulations. Herein, we performed the simulations by increasing the sizes of those NPs. In the experiments, the diameter (d) of the helical rods were kept unchanged, while the length (l) of the helical rod and the radius (r) of smooth/striped sphere were increased by nearly 1.5 times. In order to denote this change in the sizes, we also changed the sizes of NPs in simulations. For the rod-like NPs, the value of l was increased by 1.5 times, with the value of d unchanged. And for the spherical NPs, the value of r was also increased by 1.5 times. In specific, $d = 8\sigma$, $l = 48\sigma$, and $r = 12\sigma$. And the area of membrane was also increased from $70{\times}70\ \sigma^2$ to $100{\times}100\ \sigma^2$. All the other parameters were kept unchanged.

The simulation results are provided in Figure S6. It can be seen that the cellular internalization are almost the same with those of the smaller NPs in the main test. From the snapshots of the system shown in Figure S6a to 6c, it can be seen that all these NPs can be completely endocytosed. However, the endocytosis durations are much longer than those of the smaller NPs. The helical rods and striped spheres show higher internalization efficiency than the smooth sphere does. Considering the experiments in the main text, the simulations gained qualitatively consistent results with those in the experiments. And these simulations further revealed the detailed internalization processes of the three types of NPs with larger sizes.
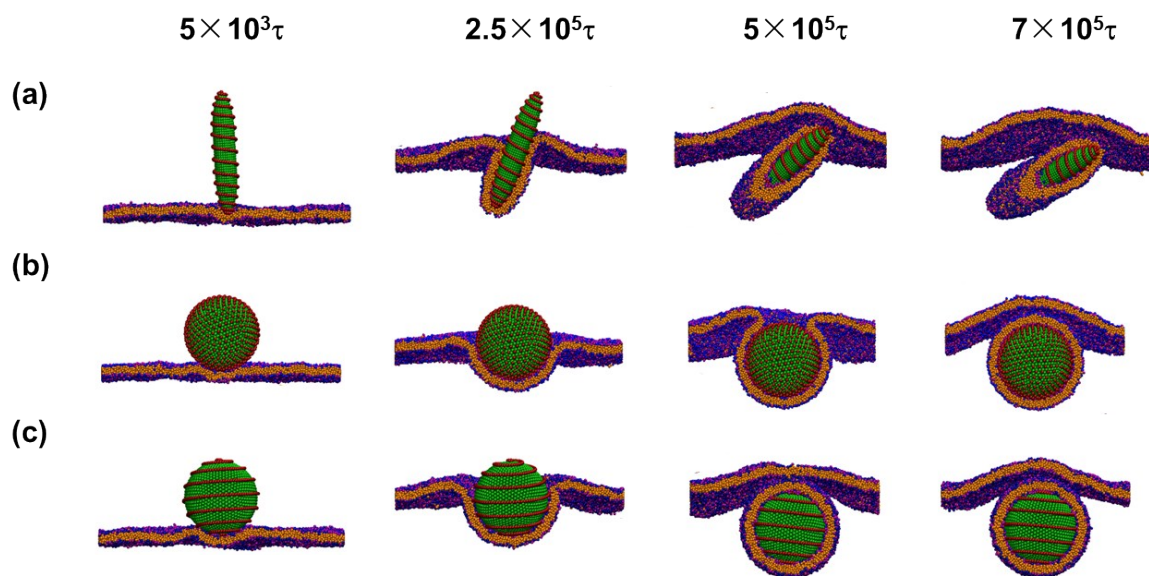
Figure S6. Snapshots during the internalization of NPs with different shapes and surface morphologies: (a) helical rod; (b) smooth sphere; (c) striped sphere.

References

S1   C. Cai, J. Lin, X. Zhu, S. Gong, and X.-S. Wang, L. Wang, *Macromolecules*, 2016, **49**, 15-22.

S2   C. Cai, Y. Li, J. Lin, L. Wang, S. Lin, X.-S. Wang, and T. Jiang, *Angew. Chem. Int. Ed.*, 2013, **52**, 7732-7736.

S3   X. Zhu, Z. Guan, J. Lin, and C. Cai, *Sci. Rep.*, 2016, **6**, 29796.

S4   W. Ding, S. Lin, J. Lin, and L. Zhang, *J. Phys. Chem. B*, 2008, **112**, 776-783.

S5   C. Cai, W. Zhu, T. Chen, J. Lin, and X. Tian, *J. Polym. Sci., Part A: Polym. Chem.*, 2009, **47**, 5967-5978.

S6   F. H. Schacher, U. Freier, and F. Steiniger, *Soft Matter*, 2012, **8**, 6968-6978.

S7   Z. Guan, L. Wang, X. Zhu, and J. Lin, *Mater. Chem. Front.*, 2017, **1**, 697-708.

S8   Z. Guan, L. Wang, and J. Lin, *Biomacromolecules*, 2017, **18**, 797-807.

S9   I. R. Cooke and M. Deserno, *J. Chem. Phys.*, 2005, **123**, 224710.

S10   R. Vácha, F. J. Martinez-Veracoechea, and D. Frenkel, *Nano Lett.*, 2011, **11**, 5391-5395.

S11   T. Schneider and E. Stoll, *Phys. Rev. B*, 1978, **17**, 1302-1322.

S12   G. S. Grest and K. Kremer, *Phys. Rev. A*, 1986, **33**, 3628-3631.

S13   G. K. Bourov and A. Bhattacharya, *J. Chem. Phys.*, 2003, **119**, 9219-9225.

S14   G. S. Grest, M. D. Lacasse, K. Kremer, and A. M. Gupta, *J. Chem. Phys.*, 1996, **105**, 10583-10594.

S15   H. J. C. Berendsen, J. P. M. Postma, W. F. van Gunsteren, A. DiNola, and J. R. Haak, *J. Chem. Phys.*, 1984, **81**, 3684-3690.

S16   C. D. Walkey, J. B. Olsen, H. Guo, A. Emili, and W. C. W. Chan. *J. Am. Chem. Soc.*, 2012, **134**, 2139-2147.

S17   X. Shi, A. von dem Bussche, R. H. Hurt, A. B. Kane, and H. Gao. *Nature Nanotech.*, 2011, **6**, 714-719.